ICHEP'98 #206
Submitted to Pa 10
Pl 12

DELPHI 98-76 CONF 144
22 June, 1998

# Analysis of the single photon channel at LEP 2



Preliminary

DELPHI Collaboration

**P. Ferrari** [1], **C. Matteuzzi** [1], **E. Falk** [2], **V. Hedberg** [2], **A. Firestone** [3], **P. Checchia** [4], **F. Mazzucato** [4]

**Abstract**

A study has been made of the production of single photons in the reaction $e^+e^- \to \gamma$ + *invisible particles* at $\sqrt{s} = 183$ GeV. The analysis uses data which correspond to an integrated luminosity of about 50 pb$^{-1}$, collected with the DELPHI detector. The number of light neutrino families is measured. The absence of an excess of events beyond that expected from Standard Model processes is used to set limits on new physics. The cross sections and masses of supersymmetric particles like neutralinos and gravitinos, for specific model parameters, are investigated. A search for a substructure as described by composite models is carried out.

Paper submitted to the ICHEP'98 Conference
Vancouver, July 22-29

[1] Sezione INFN, Milano, Italy.
[2] Lund University, Lund, Sweden.
[3] Iowa State University, Ames, USA.
[4] Sezione INFN and University of Padova, Italy.

# 1 Introduction

The process

$$e^+e^- \rightarrow \gamma + \text{invisible particles} \tag{1}$$

receives a contribution within the Standard Model from the radiative production of neutrino-antineutrino pairs through the radiative return to the $Z^0$ and the $t$-channel $W$ exchange, with the photon radiated from the beam electron or the exchanged $W$. Possible contributions to this final state could come from a new generation of neutrinos, from the radiative production of some other neutral weakly interacting particle or from a new particle decaying into a photon. Theories of supersymmetry (SUSY) predict the existence of particles, such as the neutralino, which would give origin to a final state with missing energy and a photon if the lightest neutralino decays into $\tilde{G}\gamma$ with an essentially massless $\tilde{G}$ ($m_{\tilde{G}} < 1$ eV/c$^2$). Several results have been published on this topic [1] [2].

In the study presented here, the *single* $\gamma$ + *missing energy* final state at LEPII is used to explore the existence of possible new particles. After the description of the main detectors used in the analysis and the selection criteria of the data samples (Sections 2, 3 and 4), a measurement of the number of neutrino families is made. Limits on physics beyond the Standard Model are presented in the sector on compositeness (preons) [3] and supersymmetric particles [4].

# 2 The DELPHI detector

The general criteria for the selection of events are based mainly on the electromagnetic calorimeters and the tracking system of the DELPHI experiment [5]. All three major electromagnetic calorimeters in DELPHI, the High density Projection Chamber (HPC), the Forward ElectroMagnetic Calorimeter (FEMC) and the Small angle TIle Calorimeter (STIC), have been used in the single photon reconstruction. The angular coverage of these detectors and the energy resolution are given in Table 1.

| | Angular coverage | Energy resolution |
|---|---|---|
| STIC: | $2^\circ < \theta < 10^\circ$ and $170^\circ < \theta < 178^\circ$ | $\sigma/E = 0.0152 \oplus (0.135/\sqrt{E})$ |
| FEMC: | $10^\circ < \theta < 37^\circ$ and $143^\circ < \theta < 170^\circ$ | $\sigma/E = 0.03 \oplus (0.12/\sqrt{E}) \oplus (0.11/E)$ |
| HPC: | $40^\circ < \theta < 140^\circ$ | $\sigma/E = 0.043 \oplus (0.32/\sqrt{E})$ |

Table 1: Polar angle coverage and energy resolution of the electromagnetic calorimeters in DELPHI ($E$ is in GeV).

The barrel region is covered by the HPC, which is a gas sampling calorimeter consisting of 144 modules arranged in 6 rings inside the magnetic field. Each module contains 41 layers of a lead converter with a total thickness of 18 $X_0/sin(\theta)$. In between the converter layers are slots with an argon/methane gas mixture and when ionization is produced in the gas, the detector can measure the position and energy of the shower in the same way

as a time projection chamber. A shower is sampled nine times longitudinally [5].

FEMC is made up of an array of 4532 lead glass blocks in each endcap. The 5 m diameter lead glass walls have a depth of 20 $X_0$. The blocks are truncated pyramids that give a readout granularity of about 1° both in $\phi$ and in $\theta$. The Cherenkov light produced in the lead glass by the charged particles from a shower is read out by phototriods. The energy resolution of the calorimeter is degraded by the material in front of it, which causes photon conversions and even preshowers. This degradation is particularly severe at low and high polar angles.

The very forward luminosity monitor STIC consists of two lead-scintillator calorimeters of shashlik type, read out by wavelength-shifting fibers. They are located on either side of the interaction point at a distance of 2.2 m and have a thickness of about 27 $X_0$. The tower structure is divided into ten rings and sixteen sectors for a total of 160 towers in each calorimeter. An electron veto detector, consisting of two layers of scintillator mounted on the front of each calorimeter together with a smaller ringshaped scintillator mounted directly on the beampipe, is used in the trigger to provide $e - \gamma$ separation.

In addition to the electromagnetic calorimeters, the DELPHI tracking system, which is made up of several independent detectors, is used to reject events in which charged particles are produced. The main tracking devices are the Time Projection Chamber (TPC) and the microVertex silicon Detector (VD) and its extension into the forward region, the so-called Very Forward Tracker (VFT). The two latter detectors are also used for electron/photon separation by vetoing photon candidates which can be associated with hits in these detectors.

Finally, the hadron calorimeter (HCAL) is used to reject cosmics and to provide photon/hadron separation.

## 2.1 The single photon trigger

Three different triggers are used in DELPHI to select the single photon events. It is essential for the analysis that the performance and the efficiency of these triggers are well understood.

The HPC trigger for purely neutral final states uses a plane of scintillators inserted into one of the HPC sampling gaps at a depth of around 4.5 $X_0$. A second level trigger decision is produced from the signals of analog electronics and is based on a coincidence pattern inside the HPC module. The trigger efficiency [6] has been measured with radiative events ($\mu\mu\gamma$ and $ee\gamma$) and Compton events. It is strongly dependent on the photon energy up to ∼12 GeV (Figure 1) and it varies from 40% to 80% in the interval 4 to 30 GeV and is $(89.0 \pm 2.5)\%$ for $E_\gamma > 40$ GeV . This efficiency does not include losses due to the cracks between modules of the HPC detector.

The FEMC trigger requires an energy deposition of at least 2.5 GeV. The efficiency increases with energy and is ∼97% at 18 GeV. Correlated noise in several adjacent channels

causes fake triggers, but these can be rejected offline with high efficiency by algorithms that take into account the lead glass shower pattern.

The STIC trigger requires an energy deposition of at least 15 GeV and reaches full efficiency at 30 GeV. An online angular cut to reject off-energy background restricts the acceptance to $2.6° < \theta < 9.0°$, where $\theta$ is the angle with respect to the beamline. Since the scintillator layers in front of the calorimeters are used in anti-coincidence with the calorimeter signal, electrons are rejected by the trigger. This means that photons that convert are not included in the STIC single photon sample. The trigger efficiency has been measured with a sample of photons from $e^+e^-\gamma$ events with one of the electrons seen in FEMC and the microvertex detectors and the other electron lost in the beampipe. The efficiency varies between 54% and 21% if the angular region is limited to $3.8° < \theta < 8.0°$ (Figure 1).

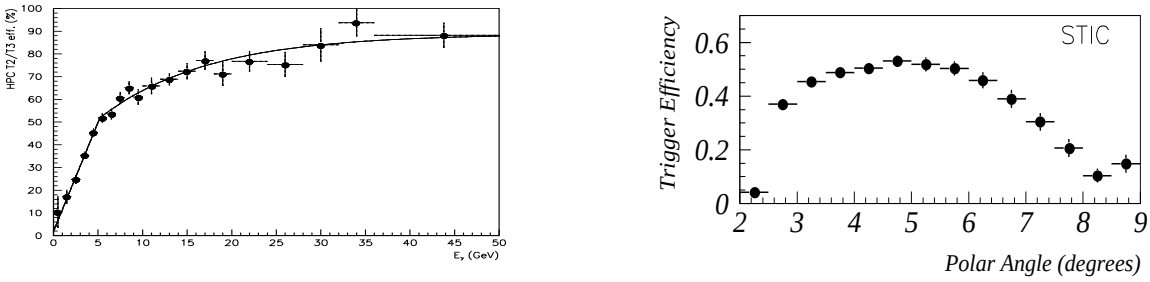


Figure 1: *LEFT* : HPC single photon trigger efficiency as a function of the photon energy. The losses due to the HPC cracks are not included. *RIGHT* : The STIC single photon trigger efficiency as a function of the polar angle.

# 3 Event and photon selection

The basic selection criteria of events are the same for the three electromagnetic calorimeters: no charged tracks detected and no electromagnetic showers apart from the shower from the single photon candidate. However, the details of the selection vary for the different electromagnetic calorimeters.

## 3.1 Photons in the HPC acceptance

Events with a photon in the HPC were selected if there were no charged particles coming from the interaction point detected in the the Time Projection Chamber. The presence of tracks in the forward region of the detector and of tracks in the TPC not coming from the interaction point was used to veto events due to background from beam gas and cosmic rays. In order to reject the background from radiative Bhabha events and Compton events, no energy deposit larger than 1 GeV in the STIC was allowed. It was also required that no other electromagnetic showers were present in the forward electromagnetic calorimeters and a second shower in the HPC was accepted only if it was within 20° of the first one. The hadronic calorimeter was used to reject cosmic events. The

event was rejected if there were two hadronic showers recorded in the HCAL. If only one shower was present, the event was retained if the HCAL shower was consistent with being caused by punch-through of the electromagnetic shower. A constraint on the $\gamma$ direction was imposed, requiring that the line of flight and the shower direction measured in the calorimeter coincided within 15°.

Only showers having an energy above 6 GeV and a polar angle in the interval $45° < \theta < 135°$ were considered. They were required to satisfy some conditions meant to define good electromagnetic shape. A shower therefore had to start in the first three rows (that is, within the first 2.0 $X_0$) and have at least three rows filled and no more than one empty row until the end of the shower development. The polar angle of the shower axis had to be outside the range 88° to 92°, where the HPC has a dead region. Finally, the shower direction had to be consistent with the $z$ coordinate, accounting for the fact that $z < 0$ is on the $\theta > 90°$ side, and $z > 0$ is on the $\theta < 90°$ side.

The photon identification efficiency depends on the criteria applied to require a good electromagnetic shower. It has been determined on the basis of a Monte Carlo sample of events passed through the complete simulation of the DELPHI detector [7]. The identification efficiency depends on the photon energy as shown in Figure 2. It ranges from ∼45% at low $E_\gamma$ to ∼78% for $E_\gamma > 15$ GeV. Figure 2 also includes the inefficiency due to the dead regions of the HPC detector.

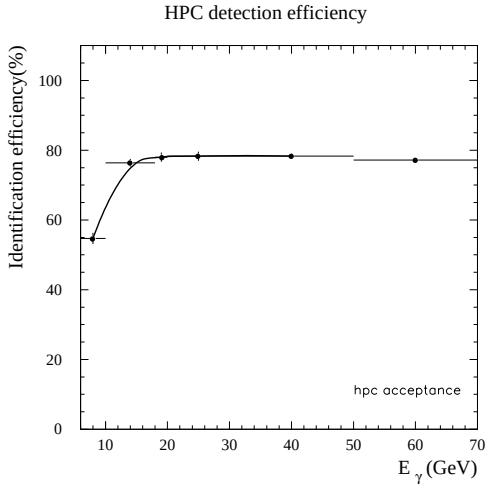


Figure 2: Efficiency of the single photon selection criteria in the HPC.

## 3.2 Photons in the FEMC acceptance

Events were preselected if they had at least one shower in FEMC with an energy above 10 GeV and a polar angle in the intervals $11° < \theta < 30°$ or $150° < \theta < 169°$. Showers in the lower and upper parts of FEMC were discarded because of the large amount of material in front of FEMC due to the STIC and the TPC detectors. In order to separate electrons from photons, the FEMC shower was extrapolated to the interaction point and the event was rejected if hits in the silicon microvertex detectors (VD and VFT) could be

associated with the shower.

The next step in the analysis was to require no charged tracks or additional electromagnetic showers in the event. However, the large amount of material in front of FEMC meant that about half of the photons preshowered before reaching the calorimeter. Most of the preshower was contained in a cone of about 12° around the largest shower and the selection took this into account by requiring no charged tracks, no electromagnetic showers (in STIC, FEMC and the HPC) and no hadronic showers outside a 12° cone. If there were no charged tracks inside the cone either, i.e., the photon had not preshowered, it was required that only one FEMC shower was present in the event. If, on the other hand, charged tracks were present in the cone, more than one FEMC shower were allowed and their momentum vectors were added to that of the largest shower.

The requirement of no electromagnetic showers outside the cone greatly reduced the background of radiative Bhabha and Compton events by rejecting events that had one or both electrons in the acceptance of the experiment. Events with hadrons and cosmics were rejected by the requirement of no hadronic showers outside the cone. In addition, it was required that the ratio of electromagnetic to electromagnetic plus hadronic energy inside the cone was larger than 0.95 .

Most reconstruction and event selection efficiencies in the analysis were taken into account by using Monte Carlo samples passed through the extensive detector simulation package of DELPHI [7]. Some efficiencies, however, were determined from data. In particular, the requirements of no electromagnetic or hadronic showers and no charged tracks were studied. A sample of events triggered at random and a sample of back-to-back Bhabha events with the electrons in STIC were used for this purpose. It was found that noise and machine background caused showers and tracks which would veto about 13% of the good single photon events.

### 3.3 Photon selection in the STIC acceptance

Single photons in STIC were selected by requiring one shower with an energy of at least 20 GeV in one of the two STIC calorimeters and no other electromagnetic showers in STIC, nor in FEMC or the HPC. No charged tracks in any of the tracking systems in DELPHI and no showers in the hadron calorimeter were allowed in the event. It was furthermore required that all single-photon candidates had satisfied the STIC single photon trigger and that there was no signal in at least one of the two large scintillator planes in front of the shower. A requirement of no signal in the small scintillators mounted on the beampipe made it possible to reject some of the radiative $ee\gamma$ background. In spite of the scintillator requirements, the huge background of off-energy electrons made it necessary to introduce the energy cut shown as a dashed line in Figure 3.

The trigger efficiency in the STIC acceptance was discussed in Section 2.1 . The offline photon identification and reconstruction resulted in an additional loss of 5% of the photons. The selection of events with no shower in STIC and no tracks introduced similar losses as those in the FEMC analysis and were estimated with the same methods.

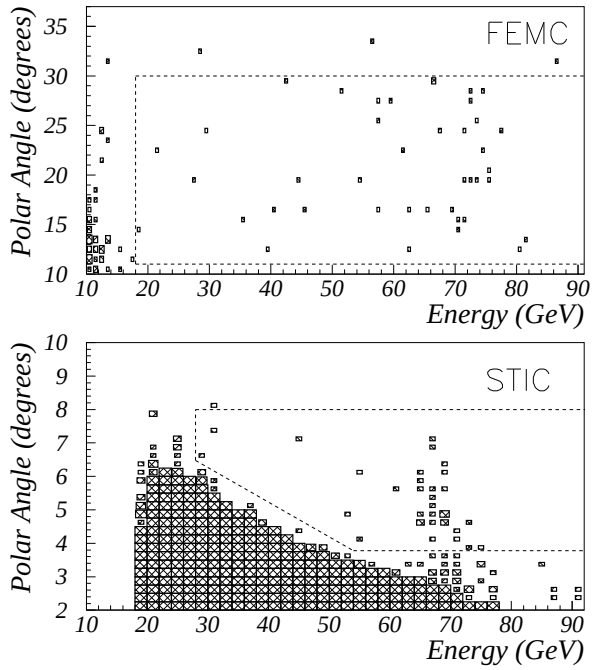


Figure 3: The polar angle versus energy distribution of photon candidates in FEMC and STIC (a full box contains five or more entries). Photons in both endcaps are shown with $\theta = 180^\circ - \theta$ for $\theta > 90^\circ$. The dashed lines indicate the regions used in the final analysis.

# 4 Background and data sample

The main source of background is the QED process $e^+e^- \to e^+e^-\gamma$ where the two electrons escape undetected along the beampipe or the electrons are lost by not being detected by the experiment. This process has a very high cross section [8], decreasing rapidly when $E_\gamma$ and the photon polar angle increase. In Figure 3, the events in FEMC at low energy and low polar angle are all due to this process. The behaviour of this QED background together with the rapidly varying efficiencies at low energies are the reasons why different energy cuts had to be applied for photons in the three calorimeters. In the final analysis it was required that $x_\gamma > 0.06$ (HPC), $x_\gamma > 0.2$ (FEMC) and $x_\gamma > 0.3$ (STIC), where $x_\gamma$ is the photon energy in units of the incident beam energy.

The critical parameter in the rejection of the $e^+e^-\gamma$ background is the polar angle at which the electrons start being detected by the experiment, i.e., seen in the STIC detector. This detector reconstructs electrons down to $\theta = 38$ mrad and in addition the scintillator counters mounted on the beampipe can be used to reject events with electrons down to 31 mrad. Simulations have shown that even at lower angles (down to 17 mrad) a large fraction of the electrons are detectable because they interact with a tungsten shield mounted inside the beampipe. Since the electrons have a high energy and the shield is thin, the electromagnetic showers leak enough energy into the STIC to make it possible

to reject the events.

The remaining background from the $e^+e^-\gamma$ process in the acceptance of the STIC and FEMC detectors was calculated with a Monte Carlo program [9] and two different event topologies were considered. Either both electrons were below the STIC acceptance or one or both of the electrons were in the DELPHI acceptance but were not detected by the experiment.The first topology gives background at low photon energy while the second one contributes photons at higher energy. The estimated number of $e^+e^-\gamma$ events with the energy cuts described previously are given in Table 2. In the HPC acceptance an analytical calculation [8] showed that the $e^+e^-\gamma$ background was negligible.

| | HPC | | FEMC | | STIC | |
|---|---|---|---|---|---|---|
| $x_\gamma$: | 0.06-0.60 | $\geq$0.60 | 0.20-0.60 | $\geq$0.60 | 0.30-0.60 | $\geq$0.60 |
| $N_{observed}$: | 16$\pm$4.0 | 38$\pm$6.2 | 15$\pm$3.9 | 43$\pm$6.5 | 4$\pm$2.0 | 24$\pm$4.9 |
| $N(e^+e^- \to e^+e^-\gamma)$: | 0 | 0 | 0.57$\pm$0.22 | 2.51$\pm$0.43 | 0.20$\pm$0.04 | 0.41$\pm$0.41 |
| $N(e \to e\gamma)$: | 0 | 0 | 0 | 0 | 0.23$\pm$0.23 | 1.38$\pm$0.56 |
| $N(e^+e^- \to \nu\bar{\nu}\gamma)$: | 23.9$\pm$0.7 | 35.6$\pm$1.0 | 12.1$\pm$1.0 | 36.0$\pm$1.7 | 2.5$\pm$0.2 | 22.2$\pm$0.9 |
| $N^{total}_{expected}$: | 23.9$\pm$0.7 | 35.6$\pm$1.0 | 12.7$\pm$1.0 | 38.5$\pm$1.8 | 2.9$\pm$0.3 | 24.0$\pm$1.1 |

Table 2: The observed and expected number of events for different processes. All errors are statistical only.

A background seen only in STIC is the single electron background produced by interactions between the beam particles and residual gas molecules in the LEP beampipe. In these $e \to e\gamma$ events the photons are always lost in the beampipe while the off-energy electrons are bent into the STIC acceptance by the low-beta quadrupoles close to DELPHI. The rate of this background is so large that in the sample of events triggered by the STIC photon trigger there were several thousands of misidentified off-energy electrons for each photon from a $\nu\bar{\nu}\gamma$ event. It was not possible to provide a $\gamma - e$ separation powerful enough to eliminate completely this background.

A detailed study (including a simulation) of off-energy electrons has been made [10]. This study showed that the off-energy background is created in different parts of LEP and then focused by the magnets into different azimuthal sectors of STIC giving rise to different radius and energy distributions depending on the origin in LEP of the $e \to e\gamma$ process. The rate of this background depends on the vacuum pressure in the LEP ring and since this vacuum pressure is not known in detail a reliable estimation of the number of background events by a simulation is not possible. Instead a background sample was collected with a trigger similar to the photon trigger but without the requirement of an absence of signal in the scintillator vetocounter. With the exception of the scintillator requirement, all cuts in the photon analysis were applied to this background sample, which contained about twice the number of events compared to the number of photon candidates. From this analysis it was established that a clean photon sample could be obtained by removing showers at low energy and low polar angle as indicated by the dashed line in

Figure 3. The remaining background in the accepted region was estimated to be 1.6±0.6 events.

Other backgrounds, such as $\gamma\gamma$ collisions, $e^+e^- \to \gamma\gamma$ and cosmic events, were found to be negligible.

The $\nu\bar{\nu}\gamma$ process was simulated by the KORALZ [11] and NUNUGPV [12] programs. The final number of expected and observed events are given in Table 2. In total, 140±12 single photon events were observed in the three calorimeters, with 138 events expected from known sources, all at 183 GeV. The energy spectrum of the selected events is shown in Figure 4 together with the expected contributions from background and $\nu\bar{\nu}\gamma$.

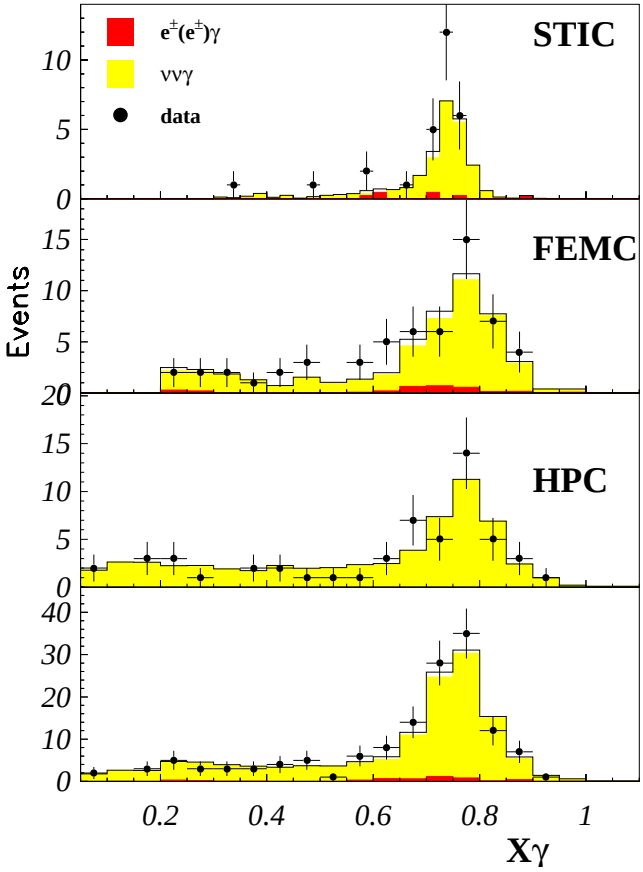


Figure 4: $x_\gamma = E_\gamma/E_{beam}$ of selected single photons in STIC, FEMC, HPC and for all calorimeters combined. The dark shaded area is the background from QED processes and the light shaded area is the expected spectrum from $e^+e^- \to \nu\bar{\nu}\gamma$ while the histogram is the sum of both.

Where relevant for the analysis, the samples in the HPC consisting of 10 events at 161 GeV and 11 events at 172 GeV were also considered (the total collected luminosity was 19.9 pb$^{-1}$). At these lower energies the number of expected events from Standard Model sources was 15.1 and 10.8 at the two energies respectively [13].

# 5 Analysis of the single photon sample

## 5.1 Cross sections

The cross sections at $\sqrt{s} = 183$ GeV after correcting for background and efficiencies are given in Table 3. Events with more than one photon contribute to the measured cross section if the other photons are at low angle ($\theta_\gamma < 38$ mrad), low energy ($E_\gamma < 1.5$ GeV) or within 3, 12 and 20 degrees with respect to the highest energy photon in STIC, FEMC and HPC respectively.

| | HPC | FEMC | STIC |
|---|---|---|---|
| $\theta_\gamma$: | $45^\circ - 135^\circ$ | $11^\circ - 30^\circ$ , $150^\circ - 169^\circ$ | $3.8^\circ - 8.0^\circ$ , $172^\circ - 176.2^\circ$ |
| $x_\gamma$: | $\geq$0.06 | $\geq$0.20 | $\geq$0.60 |
| Luminosity: | 50.2 $pb^{-1}$ | 44.3 $pb^{-1}$ | 52.0 $pb^{-1}$ |
| $\sigma(\gamma + inv.)$ | 1.85±0.25±0.15 pb | 2.26±0.31±0.18 pb | 1.09±0.21±0.12 pb |
| $\sigma(\nu\bar{\nu}\gamma)$ for $N_\nu = 3$ | 2.04 pb | 1.96 pb | 1.12 pb |
| $N_\nu$ | 2.7±0.4±0.2 | 3.5±0.5±0.3 | 2.9±0.6±0.3 |

Table 3: The corrected cross section for $e^+e^- \to \gamma + invisible$ and the calculated cross section for $e^+e^- \to \nu\bar{\nu}\gamma$. The first error quoted is statistical and the second systematic. $N_\nu$ is the number of light neutrino generations.

The contribution from various sources to the systematic error is given in Table 4. The dominant uncertainty comes from the estimation of trigger and detection efficiencies. The total systematic error is taken as the individual errors added in quadrature.

| | HPC | | FEMC | | STIC | |
|---|---|---|---|---|---|---|
| Source | Variation | $\Delta\sigma$ | Variation | $\Delta\sigma$ | Variation | $\Delta\sigma$ |
| Luminosity | ±1% | ±1% | ±1% | ±1% | ±1% | ±1% |
| Trigger efficiency | ±5% | ±5% | ±2% | ±2% | ±6% | ±6% |
| Identification efficiency | ±5% | ±5% | ±6% | ±6% | ±7% | ±7% |
| Calorimeter energy scale | ±5% | ±4% | ±5% | ±5% | ±0.5% | ±1% |
| Background | ±25% | ±1% | ±50% | ±3% | ±75% | ±6% |
| Total | | ±8% | | ±8% | | ±11% |

Table 4: Contribution to systematic errors of the cross section measurement $e^+e^- \to \gamma + invisible$.

A measurement of the cross section of the process $e^+e^- \to \nu\bar{\nu}\gamma$ makes it possible to calculate the number of light neutrino generations ($N_\nu$). DELPHI has previously reported

a value of $N_\nu = 2.89 \pm 0.32$ from LEPI data only [14]. A similar study has now been carried out with the LEPII data. In this analysis, a Monte Carlo method [12] was used to calculate the expected values of the cross section of the process $e^+e^- \to \nu\bar{\nu}\gamma$. The cross section was calculated inside the acceptance of each of the three detectors used in the analysis. Figure 5 shows the expected behaviour of the cross section, calculated with $NUNUGPV$, for three neutrino families compared with the values measured with the HPC detector at different LEP energies.

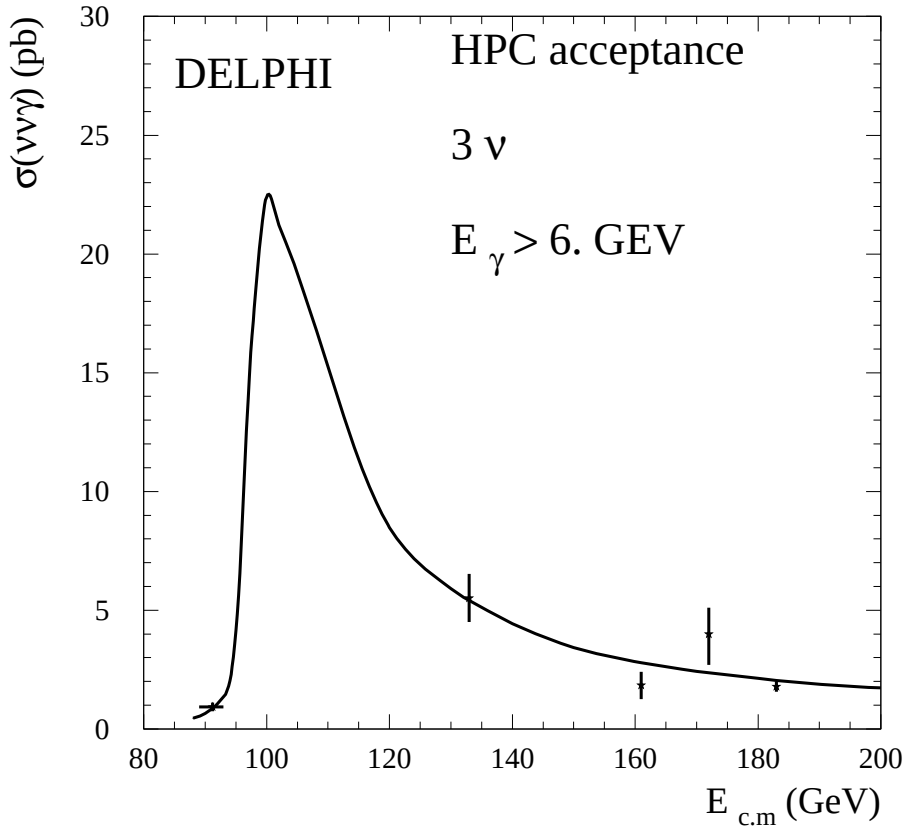


Figure 5: The measured cross sections at 91, 133, 161, 172 and 183 GeV compared to the expected $\sigma(\nu\bar{\nu}\gamma)$ as a function of $\sqrt{s}$ (for three neutrino generations).

The number of neutrino generations deduced from the cross section measurements are given in Table 3. Averaging the three independent measurements from the different calorimeters, and including also the data from the HPC at 161 and 172 GeV ($N_\nu = 2.6 \pm 0.6 \pm 0.4$), the number of light neutrino generations becomes:

$$N_\nu = 2.92 \pm 0.25(stat) \pm 0.14(syst)$$

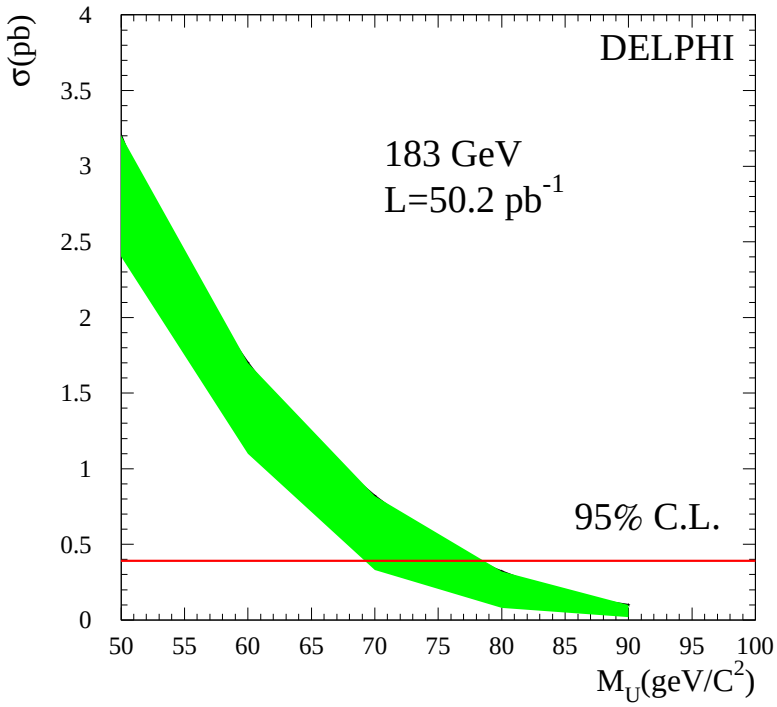


Figure 6: Limit at 95% C.L. for the mass of the $W$-type $U$ boson.

## 5.2 Limits on compositeness

Compositeness models predict several new particles which do not exist in the Standard Model. A specific Preon Model is considered in this analysis [3]. This model considers leptons, quarks and weak bosons as composite particles. Some of the predicted new particles contribute to the cross section of the process $e^+e^- \to \gamma + inv$. At a relatively light mass scale, it predicts the existence of objects connected with neutrinos $(l_S, \bar{l}_S)$, with down quarks $(q')$ and with $W$ bosons $(U^{\pm}, U^0)$. It also requires a new vector boson $D$, which could be as heavy as several times the $Z^0$ mass. The $U^0$ boson decays invisibly and can be produced in the reaction $e^+e^- \to U^0\bar{U}^0\gamma$, contributing to the process $e^+e^- \to \gamma + inv$. Also pairs of $l_S\bar{l}_S$ could be produced through $U^{\pm}$ exchange and contribute to $e^+e^- \to \gamma + inv$.

Calculating the cross sections with the hypothesis that a composite boson $D$ exists with mass between $M_D = 5 \cdot M_{Z^0}$ and $M_D = 7 \cdot M_{Z^0}$ and summing the contributions to the cross sections coming from direct production of $U^0\bar{U}^0$ pairs and the exchange of $U^{\pm}$, a limit can be obtained on $M_U$ from the measured $\sigma(e^+e^- \to \gamma + inv.)$ after subtracting the contribution expected from neutrino production in the Standard Model. The limit calculated from the HPC and FEMC data is shown in Figure 6 and it ranges between

$$M_U > 68 - 78 \text{ GeV/c}^2 \quad \text{at 95\% C.L.}$$

varying $M_D$ in the range indicated above. Weaker limits have been determined at lower LEPII energies [2].

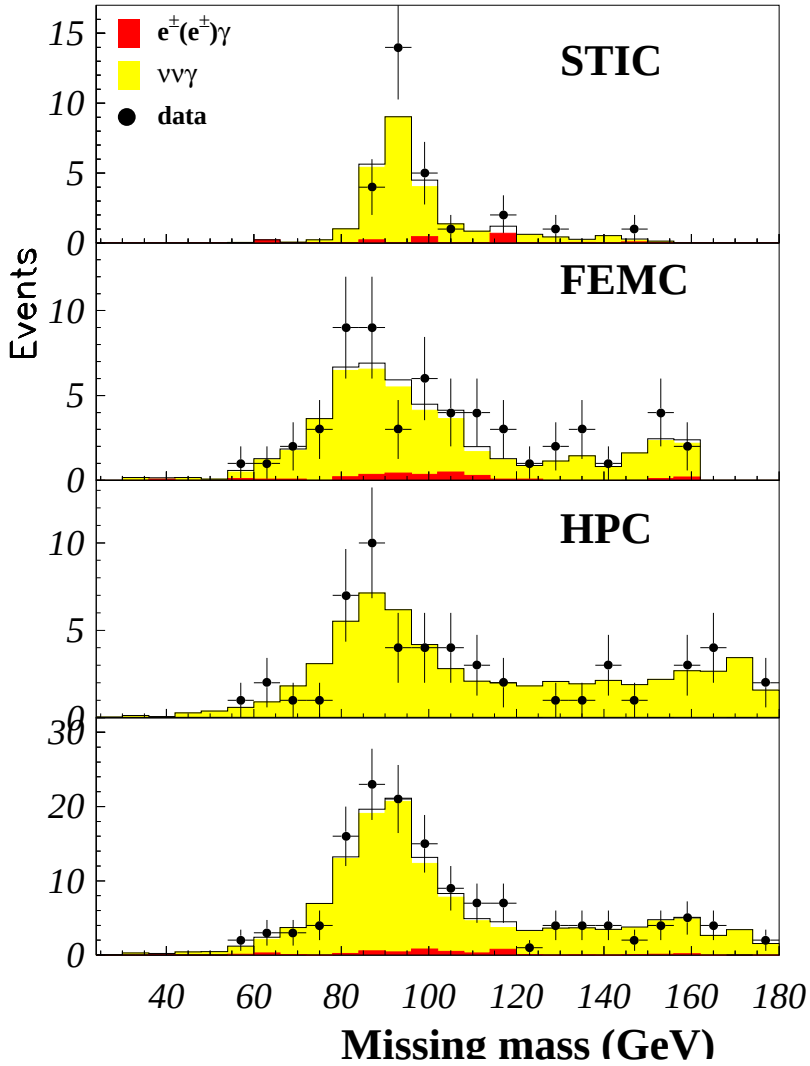


Figure 7: Distribution of the recoiling mass against the detected photon. The dark shaded area is the background from QED processes and the light shaded area is the expected spectrum from $e^+e^- \to \nu\bar{\nu}\gamma$ while the histogram is the sum of both.

## 5.3 Limits on the production of an unknown neutral state

In many previous analyses [2] [14] [15] one has used the observed candidates to set a limit on the probability of the existence of a new particle, X, produced in association with a photon and being stable or decaying to invisible decay products. The limit is calculated from the recoil mass distribution (Figure 7) of the 140 single $\gamma$ in the angular region $3.8^\circ < \theta < 176.2^\circ$ and taking into account the expected background. The limit is valid when the intrinsic width of the X particle is negligible compared to the detector resolution (the recoil mass resolution varies between 10 GeV at the $Z^0$ peak to 1 GeV at high masses). The upper limit at the 95% confidence level of the cross section for $e^+e^- \to \gamma$+X is given in Figure 8 for photons in the HPC region and in all three calorimeters. In the latter case an assumption of an ISR-like photon angular distribution has been made to correct for losses between the calorimeters.

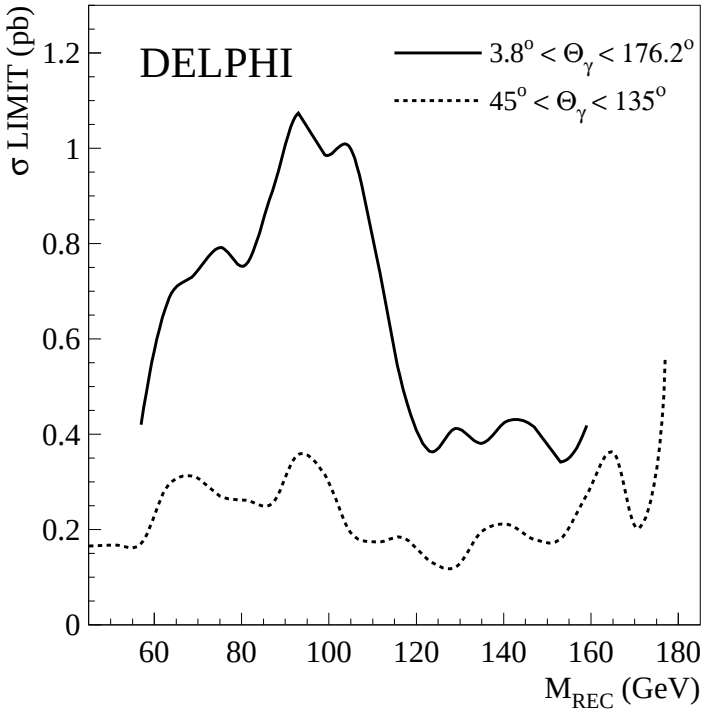


Figure 8: Limit at 95% C.L. for the production of a new unknown stable neutral object.

## 5.4 SUSY particles

### 5.4.1 Limits on the gravitino mass

Recently, the possibility of detecting a light gravitino in accelerator experiments was studied in detail [16] and the cross section for the process $e^+e^- \to \tilde{G}\tilde{G}\gamma$ was computed under the assumption that all other supersymmetric particles are too heavy to be produced. The radiative double differential cross section $d^2\sigma/(dx_\gamma, dcos\theta_\gamma)$, where $x_\gamma$ and $\theta_\gamma$ are the fraction of the beam energy carried by the photon and the photon polar angle with respect to the electron direction, is given in [16] for the radiative production ($e^+e^- \to \tilde{G}\tilde{G}\gamma$) of an undetectable gravitino pair. The total cross section can be written as:

$$\sigma = \frac{\alpha_s^3}{320\pi^2|F|^4} \cdot I, \tag{2}$$

where $|F|^{\frac{1}{2}}$ is the supersymmetry-breaking scale which is related to the gravitino mass by $|F| = \sqrt{3/8\pi} \cdot G_N^{-\frac{1}{2}} \cdot m_{3/2}$ and $I$ is an integral over the photon energy and polar angle. The largest sensitivity is obtained with photons at low energy and/or low polar angle, as illustrated by Figure 9.

Single photon final states from the Standard Model process $e^+e^- \to \nu\bar{\nu}\gamma$ have a polar angle distribution similar to the signal, except for the enhanced characteristic peak due to the radiative return to the $Z^0$, at $x_\gamma = 1 - {M_Z}^2/s$. Therefore, the optimal kinematical region in which to look for the signal is in the low region of the photon energy spectrum. Since the signal cross section (2) grows as the sixth power of the center-of-mass energy, the highest sensitivity is found at the highest beam energy. For this reason, the data taken in 1997 at $\sqrt{s} = 183$ GeV provide the best sample in which to look for the $e^+e^- \to \tilde{G}\tilde{G}\gamma$

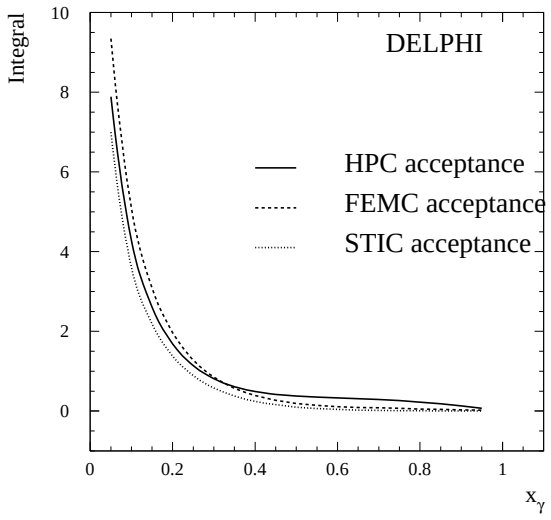


Figure 9: The behaviour of the integral $I$ (used in equation (3)) as a function of $x_\gamma$.

signal. The lower limit on the gravitino mass can be extracted from the upper limit $\sigma_0$ on the production cross section (2) through:

$$m_{3/2} > 3.8 \cdot 10^{-6} eV \left[\frac{\sqrt{s}(GeV)}{200}\right]^{3/2} \left[\frac{I}{\sigma_0}\right]^{1/4} \tag{3}$$

All the three DELPHI calorimeters, STIC, FEMC and the HPC, were used in this analysis. The sensitivity was optimized for each of them, maximizing the value of the function $I$ given in Figure 9. The different energy regions with the corresponding expectations from the Standard Model are summarised in Table 5.

| Detector | HPC | FEMC | STIC |
|---|---|---|---|
| $x_\gamma$ | 0.06-0.60 | 0.20-0.60 | 0.30-0.60 |
| $N_{observed}$ | 16 | 15 | 4 |
| $\sigma_0$ | 0.30 pb | 0.52 pb | 0.37 pb |
| $m_{3/2} >$ | $6.9 \cdot 10^{-6}$ eV | $4.6 \cdot 10^{-6}$ eV | $3.2 \cdot 10^{-6}$ eV |

Table 5: The limits on $m_{3/2}$ (as defined by equation (3)), calculated with the data from the three calorimeters.

The upper limit at 95% confidence level is calculated according to [17]. Combining the three calorimeters, one obtains the limit

$$\sigma_0 < 0.50 \text{ pb} \quad \text{at } 95\% \text{ C.L.} \tag{4}$$

The total kinematical region corresponds to $I = 7.7$ and the lower limit on the gravitino mass from equation (3) then becomes

$$m_{3/2} > 6.6 \cdot 10^{-6} \text{ eV/c}^2 \quad \text{at } 95\% \text{ C.L.} \tag{5}$$

which correspond to a SUSY breaking energy scale $|F|^{\frac{1}{2}} > 166$ GeV. The effect of the systematic uncertainties on this limit is negligible. This limit is weaker than those obtained at $p\bar{p}$ machines [18] and by astrophysical constraints [19] and it is at the same level as those set by $(g-2)_\mu$ [20]. However, it has the feature of being valid when all the masses in the SUSY models are very large.

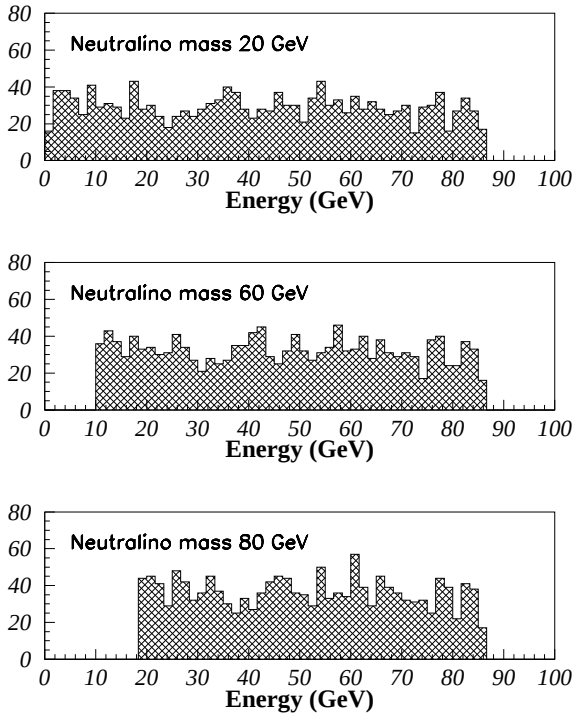


Figure 10: Energy distributions of the photon from neutralino decays produced in the process $e^+e^- \to \tilde{G}\chi \to \tilde{G}\tilde{G}\gamma$. The plots have been produced at $\sqrt{s}$ =172 GeV.

### 5.4.2 Limits on neutralino production

The production of a neutralino $\tilde{\chi}^0$ together with a gravitino $\tilde{G}$ through $e^+e^- \to \tilde{G}\tilde{\chi}^0 \to \tilde{G}\tilde{G}\gamma$ has also been considered. The limit is calculated from the energy distribution of the expected events, generated with *SUSYGEN* [21] and the observed 75 single photon events (at 161, 172 and 183 GeV) in the angular region $45° < \theta < 135°$, after taking into account the expected background from $\nu\bar{\nu}\gamma$. Figure 10 shows the expected photon energy distributions for neutralinos with different masses. The cut on $E_\gamma$ was made in such a way as to keep at least 90% of the signal. The resulting overall efficiency including both the energy cut and the geometrical acceptance was 66%. The calculated upper limit for the cross section of the process $e^+e^- \to \tilde{G} + \tilde{\chi}^0$ is given in Figure 11 for the data at 183 GeV.

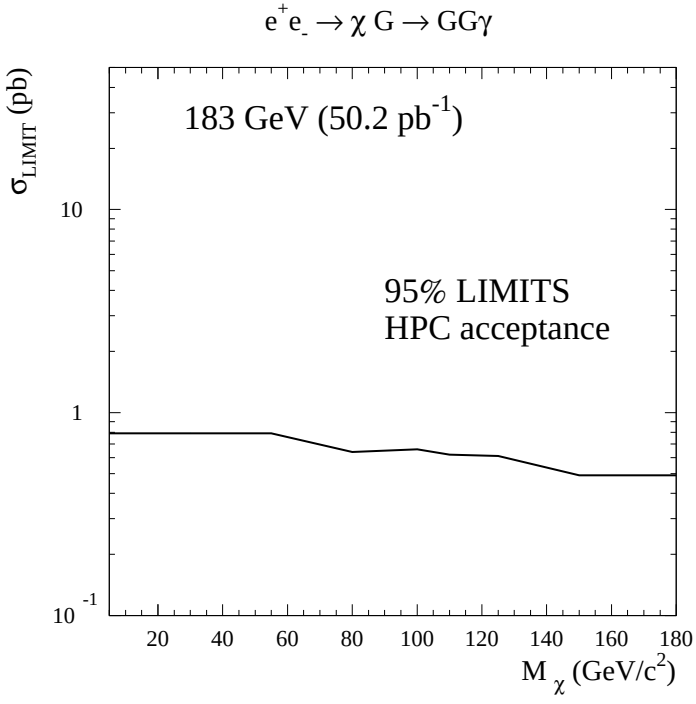


Figure 11: Upper limits for the cross section of the process $e^+e^- \to \tilde{G}\tilde{\chi} \to \tilde{G}\tilde{G}\gamma$ at 95% C.L.

# 6 Conclusions

With the 50 pb$^{-1}$ of data collected by DELPHI in 1997 at a center-of-mass energy of 183 GeV a study has been made of the production of events with a single photon in the final state and no other visible particles.

The measured cross sections are in agreement with the expectations from the Standard Model process $e^+e^- \to \nu\bar{\nu}\gamma$ and a calculation of the number of light neutrino families gives the result:

$$N_\nu = 2.92 \pm 0.25(stat) \pm 0.14(syst)$$

The absence of an excess of events has been used to set limits on the production of a new unknown model-independent neutral state, a W-type $U$-boson as described by a compositeness model, a light gravitino and neutralinos.

# References


[1] ALEPH Collaboration, R. Barate *et al.*, Phys. Lett. **B420** (1998) 127.
L3 Collaboration, M. Acciarri *et al.*, Phys. Lett. **B411** (1997) 373;
OPAL Collaboration, K. Ackerstaff *et al.*, Eur. Phys. J. C2(1998) 607.

[2] DELPHI Collaboration, P. Abreu *et al.*, Phys. Lett. **B380** (1996) 471.

[3] H. Senju, Prog. Theor. Phys. **95** (1996) 455 and references therein.

[4] S. Ambrosanio and B. Mele, Phys. Rev. **D52** (1995) 3900;
S. Ambrosanio *et al.*, Nucl. Phys. **B478** (1996) 46.

[5] DELPHI Collaboration, P. Abreu *et al.*, Nucl. Inst. and Meth. **A378** (1996) 57;
DELPHI Collaboration, P. Aarnio *et al.*, Nucl. Inst. and Meth. **A303** (1991) 233.

[6] D. Gillespie and T. Malmgren, DELPHI 94-46 CAL 155;
S. Paiano and A. Perrotta, DELPHI 98-37 CAL 139.

[7] DELPHI Collaboration, DELPHI 89-67 PROG 142;
DELPHI Collaboration, DELPHI 89-68 PROG 143.

[8] M. Caffo, R. Gatto and E. Remiddi, Phys. Lett. **B173** (1986) 91;
M. Caffo, R. Gatto and E. Remiddi, Nucl. Phys. **B286** (1987) 293.

[9] D. Karlen, Nucl. Phys. **B289** (1987) 23.

[10] E. Falk, V. Hedberg and G. von Holtey, CERN SL/97-04(EA) and DELPHI 97-12 LEDI 8.

[11] S. Jadach *et al.*, Comp. Phys. Comm. **66** (1991) 276;
S. Jadach *et al.*, Comp. Phys. Comm. **79** (1994) 503.

[12] G. Montagna *et al.*, Nucl. Phys. **B452** (1995) 161.

[13] DELPHI Collaboration, P. Abreu *et al.*, Eur. Phys. J. C1(1998) 1.

[14] DELPHI Collaboration, P. Abreu *et al.*, Z. Phys. **C74** (1997) 577.

[15] OPAL Collaboration, R. Akers *et al.*, Z. Phys. **C65** (1995) 47.

[16] A. Brignole, F. Feruglio and F. Zwirner, Preprint hep-ph/9711516.

[17] R.M. Barnett *et al.*, Phys. Rev. **D54**, 1 (1996) 166.

[18] D. Dicus and S. Nandi, Phys. Rev. **D56** (1997) 4166;
A. Brignole *et al.*, Preprint hep-ph/9801329.

[19] J.A. Grifols, Preprint hep-ph/9804225.

[20] F. Ferrer and J.A. Grifols, Phys. Rev. **D56** (1997) 7466;
T. Li, J.L. Lopez and D.V. Nanopoulos, Preprint hep-ph/9704439.

[21] S. Katsanevas and P. Morawitz, Preprint hep-ph/9711417.